Geothermics 96 (2021) 102212

Contents lists available at ScienceDirect

Geothermics

journal homepage: www.elsevier.com/locate/geothermics

An update of second law analysis and optimization of a single-flash geothermal power plant in Dieng, Indonesia

Bayu Rudiyanto [a,#,*], Muhamad Aries Bahthiyar [b], Nugroho Agung Pambudi [c], Widjonarko [d], Miftah Hijriawan [e]

[a] Energy Engineering Laboratory, Department of Renewable Energy Engineering, Politeknik Negeri Jember, Tegalgede, Jember 68121, Indonesia
[b] Graduate School of Department of Renewable Energy Engineering, Politeknik Negeri Jember, Tegalgede, Jember 68121, Indonesia
[c] Energy Society and Laboratory, Mechanical Engineering Education, Universitas Sebelas Maret, Jl. Ir. Sutami 36A, Surakarta 57126, Indonesia
[d] Department of Electrical Engineering, Universitas Jember, Jl. Kalimantan 37 Kampus Tegalboto, Jember, 68121, Indonesia
[e] Graduate Programme of Mechanical Engineering, Universitas Sebelas Maret, Jl. Ir. Sutami 36A, Surakarta 57126, Indonesia

ARTICLE INFO

Keywords:
Thermodynamic
Single-flash
Exergy
Power plant
Optimization

ABSTRACT

Dieng geothermal power plant is one of the Geothermal plants located in Indonesia with a total estimated potential of 400 MWe. The reservoir is characterized by water-dominated with 240 to 333°C temperature. Recently, the company operated one unit of single-flash system with a capacity of 60 MW. To improve its capacity, unit expansion of unit 2 and 3 are designed with each capacity of 60 MW. Apart from this expansion, another effort is optimizing the existing plant. It can be conducted with a thermodynamic approach using energy and exergy analysis. Therefore, this study aims to evaluate and optimize the existing geothermal power plant using energy and exergy analysis. With the latest data obtained, the results show that the exergy value of production wells is around 106,515 kW. The electricity production with the system is around 40,680 kW, resulting in an exergy efficiency of about 38.19%. Furthermore, the optimization is carried out on the turbine because it shows the greatest irreversibility of 11,217 kW. Optimization is done by varying the incoming turbine pressure. These results indicate that higher inlet pressure increases irreversibility and lowers energy efficiency. Furthermore, the optimum inlet turbine pressure is achieved at 5.5 bar with the maximum change depending on the ambient temperature.

1. Introduction

Dieng geothermal power plant is one of the Geothermal Working Areas in Indonesia with a total estimated potential of 400 MWe [1]. Furthermore, it characterized by a water-dominated reservoir with temperatures ranging from 240-333°C [1–5]. Recently, the company operated one unit of the single-flash cycle with a capacity of 60 MW [1, 6]. To improve its capacity, unit expansion of unit 2 and 3 are designed with each capacity of 60 MW. Apart from this expansion, another effort that can be performed is to evaluate and optimize the existing plant of the first unit. It can be conducted with a thermodynamic approach using energy and exergy analysis.

Energy analysis relies on the first thermodynamics law, while the exergy is based on the second law. The exergy analysis investigates irreversibility by measuring energy quality since the energy transformation causes changes in the quality, measured as exergy parameters [7–10]. The results will provide a clear picture of the system loss, the causes, as well as the location to be improved either at the overall performance or only on its components [9, 11–13].

Several researchers have conducted energy and exergy analyses of the geothermal power plant. Pambudi et al. led the first exergy analysis and optimization at Dieng geothermal power plant in 2014, which has an exergy value from the production well are estimated at 59.52 MW, with the second law efficiency being 36.48%, and optimizes the separator pressure [14]. Further research was conducted in 2015 by analyzing the performance improvement using three development scenarios and found a 19.7% increase in power output with the double-flash system configuration [15]. Moreover, another research in a different location is conducted in Kamojang, Indonesia, by analyzing the effect of ambient temperature on the exergy efficiency, optimizing the condenser because its irreversibility is the highest [16]. In the exact location in

* Corresponding author.
# ORCID: 0000-0002-4708-629X
E-mail address: bayu_rudianto@polije.ac.id (B. Rudiyanto).

https://doi.org/10.1016/j.geothermics.2021.102212
Received 5 March 2021; Received in revised form 12 July 2021; Accepted 18 July 2021

Nomenclature

$\dot{m}$	mass flow rate, kg/s
P	pressure, bar
T	temperature, ℃
$\dot{E}$	energy flow rate, kW
h	Enthalpy, kJ/kg
s	Entropy, kJ/kg.K
η	Thermal efficiency, %
W	net work, kJ
Q	heat transfer, kJ
X	quality of the fluid, %

Subscript

state	conditions being analyzed
thermal	thermal state
Input	input conditions
output	output conditions
Exergy	geothermal power plant exergy
System	geothermal power plant system
0	environment
1	production well
2	separator
3	steam line
4	scrubber
5	scrubber
6	demister
7	turbine
8	main condenser
9	hot well pump
10	hot well pump
11	scrubber
12	scrubber
13	main condenser
14	1st steam ejector
15	intercondenser
16	2nd steam ejector
17	aftercooler
18	hot well pump
19	blow down pump
20	cooling tower
21	cooling tower
22	cooling tower
23	vacuum pump
24	cooling tower
25	auxiliary pump
26	intercondenser
27	aftercooler
28	environment
29	cooling tower
30	separator
31	flasher
32	flasher
33	CDP
34	scrubber

Measurement units

kW	kilowatts
MW	megawatts
MWe	megawatts electric
kPa	kilopascal
Psi	pounds per square inch
bar	bar
Hz	hertz

Abbreviations

EES	engineering equation solver software
ORC	organic rankine cycle
AFT	atmospheric flash tank
CDP	condensate drop pot
HWP	hot well pump
BDP	blow down pump
VP	vacuum pump
AP	auxiliary pump
NCG	non-condensable gas

Kamojang, Setyawan et al. conducted an exergy analysis of the geothermal power plant in Kamojang unit 2, which has the second law efficiency of 40.31% [17].

Similar research related to energy and exergy analysis as well as optimization of geothermal power plants has also been carried out at various sites in the world. Unverdi and Cerci conduct the efficiency of exergy in Germencik Geothermal Power Plant, which has a power output of 47.4 MWe [18]. In comparison, Yari studied the different geothermal power plant concepts based on the exergy analysis for high-temperature geothermal resources [19]. Besides, Ghazvini et al. conducted a review of hydrogen production using geothermal energy, where the cost is lower than other energies. From an environmental perspective, hydrogen production using geothermal energy results in much lower carbon dioxide production than other renewable energy sources and fossil energy [20].

Further, with exergy analysis, Koroneos et al. conducted an exergy analysis to determine the technical appropriateness of developing a geothermal power plant in Binary on Nisyros Island [21]. Moreover, DiPippo conducted an exergetic study and optimization of a double-flash geothermal power plant with interstage reheating [22]. Jalilinasrabady et al. conducted flash cycle optimization of the Sabalan geothermal power plant employing the exergy concept [23]. While Mohammadzadeh et al. conducted a classification of geothermal in Indonesia using the exergy concept [5]. Dagdas, Ozt, and Bekdemir, conducted a thermodynamic evaluation of the Denizli Kizildere geothermal power plant. The optimum flashing pressure is found to be 200 kPa [24]. Coskun, Oktay, and Dincer also performed an operational 7.5 MWe binary geothermal power plant in Tuzla, Turkey, which found that the energy and exergy losses occur in the brine reinjection unit [25]. Furthermore, Basogul conducted an environmental assessment of a binary geothermal sourced power plant using exergy analysis [26].

Researchers also use energy and exergy analysis to develop a hybrid system between geothermal resources and other renewable energy, i.e., the sun [27]. Gokgedik, Yurusoy, and Kecebas improved a real geothermal power plant using advanced exergy analysis, which received an efficiency increase of 15.40% by improving all components [28]. Besides, Yuksel, Aslan, and Akyol investigated seasonal variation in the energy and exergy performance of the Gonen geothermal district heating system, where the annual average energy and exergy efficiency are obtained 41.07% and 45.86%, respectively. [29]. Moreover, Budisulistyo and Krumdieck conducted a pre-feasibility design investigation for a binary geothermal power plant using a typical geothermal resource in New Zealand [30]. While Atiz et al. conducted the working fluid selection that affected the performance Organic Rankine Cycle (ORC), the waste heat extracted from the ORC was used efficiently for space heating [31].

The literature review and previous research show that exergy analysis is a powerful tool for evaluating and optimizing geothermal and

thermal systems. In this research, the case study at the Dieng geothermal power plant, Indonesia, was re-appointed using the latest data. The analysis is carried out on the main components of the power plant to identify the biggest losses. Then it is used to optimize and improve the current performance of the site using EES to obtain results that are more relevant to current conditions.

2. Geothermal Energy in Dieng

2.1. Brief Description of Geothermal Energy in Dieng

Based on sub-surface research, the total potential of geothermal energy in Dieng is estimated to be 400 MWe [1], as shown in Fig. 1. The company operates the Dieng Unit 1 plant with a capacity of 60 MW. There are 46 geothermal wells available, including production and injection. Due to limitations and damage to the reservoir and wells, some wells cannot produce steam. Therefore, only seven wells are operated as a steam supply source, namely, HCE-28A, HCE-30, HCE-31, HCE-29, HCE-7A, HCE-7B, and HCE-7C with a power production capacity installed at 60 MW. Its depth average is 2500-3000 meters, with each well consisting of different pressures ranging from 300-400 Psi with the ability to produce steam at various capacities.

2.2. Description of State and Dieng Geothermal Power Plant System Data

The Dieng plant comprises main components, including a separator, scrubber, demister, turbine, main condenser, inter-condenser, aftercooler, cooling tower, and atmospheric flash tank (AFT). It also has supporting components such as Condensate Drop Pot (CDP), 1st steam ejector, 2nd steam ejector, Hot Well Pump (HWP), Blow Down Pump (BDP), Vacuum Pump (VP), Auxiliary Pump (AP), and brine booster pump.

The fluid is generated from 4 production wells, including PAD 7B, PAD 28A, PAD 30, and PAD 31. The power plant is also a mixture of brine and steam phases with a small non-Condensable Gas (NCG). A separator is used to separate each well, flowing to the flasher and ponds to lower the temperature before injecting it into the reservoir. Then, the steam generated is combined with those from other wells through the gathering system sent to the power plant. The scheme of the gathering system at the Dieng geothermal power plant is shown in Fig. 2.

In this study, the scheme of the geothermal power plant (Fig. 1) is modeled with one production well to facilitate the analysis. The pressure and temperature are the averages at each production well, while the mass flow rate is the total mass flow rate of the four wells.

A total of 34 states were analyzed and symbolized by numbers to facilitate analysis. State 0 is an ambient condition used as a dead state system in conducting an exergy analysis. State 1 is a working fluid mixture of water and steam from a production well used as an energy source to produce electricity. However, it is dominated by water, consisting of an average steam fraction of 37.32%, and separated with a separator.

State 2 is a fluid with a steam phase resulting from the separation process sent to the plant through a steam pipe by ± 4.6 km. The long distance between the production well and the powerhouse causes 5.89% of the mass flow rate of steam to become condensate due to friction. This condensate falls due to differences in density and is trapped into the CDP, which is discharged into the environment. This process causes a drop in the steam entering the scrubber, decreasing its pressure at state 3.

State 4 is the scrubber output that flows to the demister and ejectors as motive steam. State 5 is the steam from the scrubber to the demister, which passes through a filter. State 6 is the output stream from the demister which enters the turbine. The steam is dry due to the filtering process. Based on interviews with the plant operator, the demister was recently added a few years ago to prolong the turbine's lifetime since the solid particles in the steam tend to damage the filters. Furthermore, state 7 is the condensed turbine output, while state 8 is the compressed liquid inhaled by an HWP that consumes 1050 kW of electrical power. State 9 is the HWP output condensate to flow partly to the cooling tower and BDP. The HWP process is assumed to occur isentropically or fixed entropy, while state 10 is a condensate sprayed on the cooling tower through the nozzle.

State 11 and 12 are motive steam of the 1st and 2nd ejectors derived from scrubbers. Although it comes from a scrubber or state 4, the

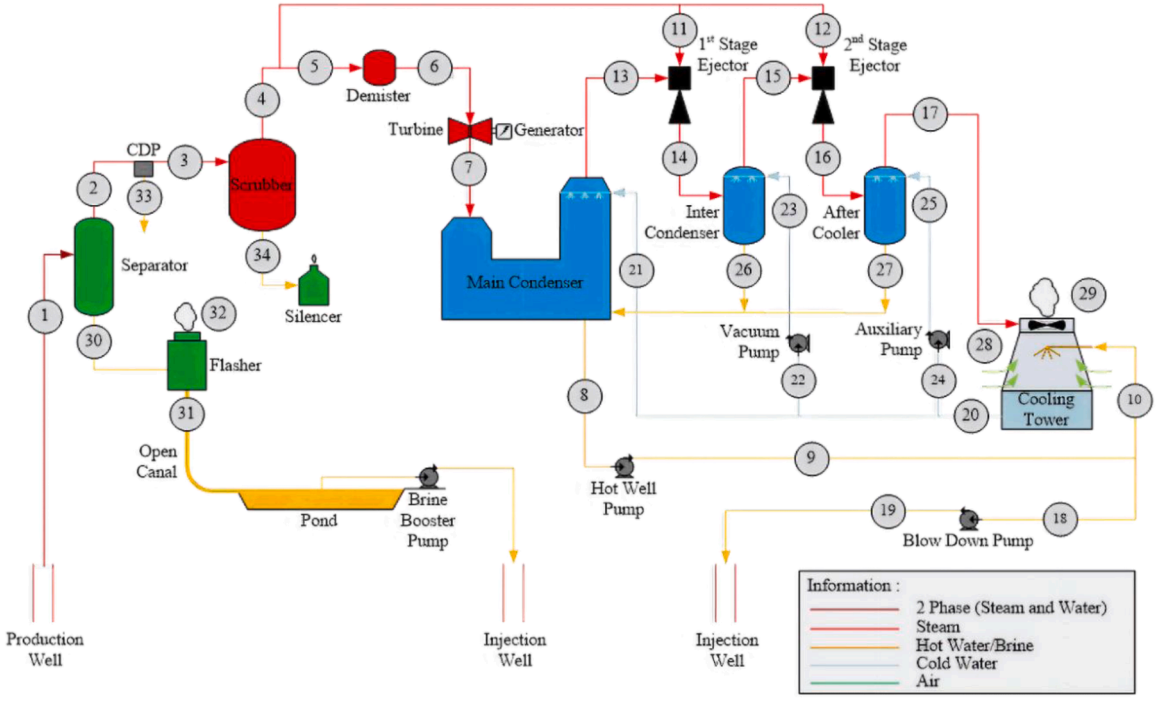

Fig. 1. The Geothermal Power Plant System schematic in Dieng consists of the separator, scrubber, demister, turbine, main condenser, inter-condenser, aftercooler, cooling tower, and flasher.

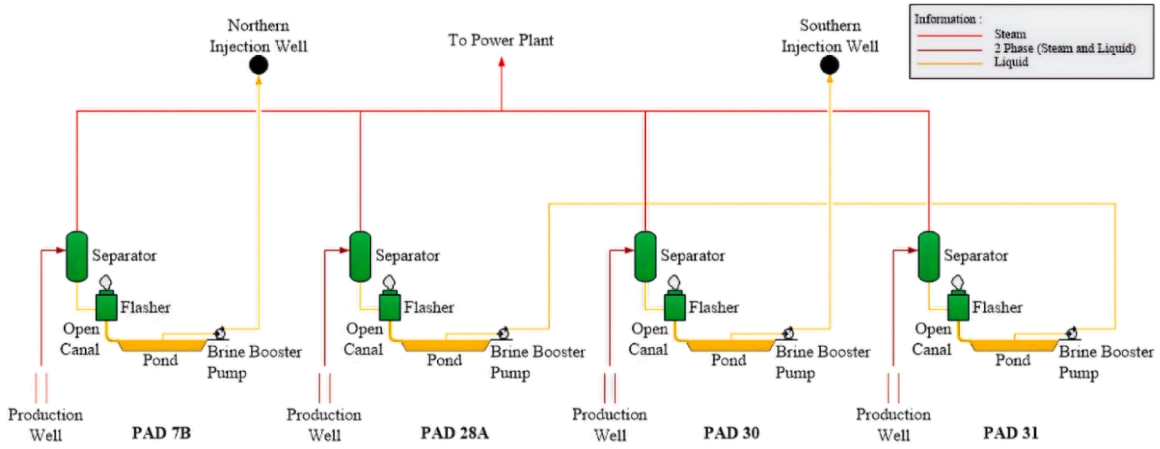

Fig. 2. Gathering System of Dieng geothermal power plant

pressure values at these states differ from state four due to the difference in the diameter of the steam pipe. Furthermore, state 13 is NCG with a portion of water steam from the main condenser inhaled by the 1st steam ejector. Also, state 14 is a mixture of motive steam with NCG, which flowed into the inter-condenser. While state 15 is an NCG and water steam from the inter-condenser inhaled by the 2nd ejector. State 16 is a mixture of motive steam, NCG, and water steam that flowed and condensed into the aftercooler. Furthermore, state 17 is a mixture of NCG and a portion of water steam flowed to the top of the cooling tower and discharged into the environment.

State 18 is part of the HWP condensate adsorbed by BDP with an electrical capacity of 149.1 kW to maintain the cooling tower level. While state 19 is the BDP condensate output that flows to the injection well. The process of BDP is assumed to occur isentropically. State 20 consists of water from the cooling tower for the condensation process, while state 21 is sprayed to condense the turbine output steam. State 22 is water from the cooling tower adsorbed by a vacuum pump which consumes 11.19 kW of electric power. While state 23 is the output water of the vacuum pump sprayed into the inter-condenser for the condensation process. The process in the vacuum pump is also assumed to occur isentropically. State 24 is water from a cooling tower supported by an auxiliary pump that consumes an electric power of 14.91 kW. State 25 is supplementary pump output water that is sprayed into the inter-condenser for condensation. The process is also assumed to occur

Table 1
Operation Data of Each State.

Component	State	$\dot{m}$ kg/s	P bar	T °C	X %	h kJ/kg	s kJ/kg.K	Energy kW	Exergy kW
Environment	0		0.78 [32]	18 [32]		75.54	0.2676		
Production Well	1	250.5	11.5		0.3732	1534	3.818	384226	106515
Separator	2	93.48	11		0.9411	2663	6.295	248980	77947
Steam Line	3	87.97	8.31		0.9992	2769	6.646	243583	73650
Scrubber	4	87.9	8.28	170.9	1	2770	6.651	243519	73596
Scrubber	5	84.66	8.28	170.9	1	2770	6.651	234533	70881
Demister	6	84.66	7.5	155.5	1	2766	6.684	234189	69705
Turbine	7	84.66	0.078	40.71	0.8567	2231	7.14	188871	13171
Main Condenser	8	2829		36.95	0	154.7	0.5313	437714	6904
Hot Well Pump	9	2829	2.94	36.95		155	0.5313	438534	7723
Hot Well Pump	10	2800	2.94	36.95		155	0.5313	434126	7646
Scrubber	11	1.684	7.58		1	2767	6.681	4659	1389
Scrubber	12	1.56	7.58		1	2767	6.681	4316	1287
Main Condenser	13	1.609	0.078	33.22	0.8567	2214	7.254	3562	170
1st Steam Ejector	14	3.293	0.571		0.7	2497	7.117	8222	1409
Intercondenser	15	0.9694	0.571	45	0.7	1864	5.906	1807	143.4
2nd Steam Ejector	16	2.529	0.945		0.7	2421	6.699	6123	1198
Aftercooler	17	0.9415	0.945	45	0.7	1864	5.906	1755	139.3
Hot Well Pump	18	28.43	2.94	36.95		155	0.5313	4408	77.63
Blow Down Pump	19	28.43	20.6	33.22		156.8	0.5313	4458	128.1
Cooling Tower	20	2742		23	0	96.39	0.3388	264256	309.7
Cooling Tower	21	2641		23	0	96.39	0.3388	254544	298.3
Cooling Tower	22	57.81		23	0	96.39	0.3388	5572	6.531
Vacuum Pump	23	57.81	1	23		96.48	0.3388	5578	12.16
Cooling Tower	24	42.95		23	0	96.39	0.3388	4140	4.852
Auxiliary Pump	25	42.95	1.42	23		96.53	0.3388	4146	10.84
Intercondenser	26	60.14		45	0	188.4	0.6385	11331	295.9
Aftercooler	27	44.54		45	0	188.4	0.6385	8391	219.2
Environment	28	66.43	0.78	18		75.54	0.2676	5018	0
Cooling Tower	29	66.43	0.78	26.5	1	2549	8.524	169340	4705
Separator	30	157	11		0	781.4	2.179	122693	23481
Flasher	31	128.8	0.78	88.25	0	369.6	1.172	47586	3962
Flasher	32	28.26	0.78	88.25	1	2657	7.501	75091	13463
CDP	33	5.506	8.31	174.5	0.0589	848.5	2.332	4672	947.6
Scrubber	34	0.07038	8.28	170.9	0.0008	729.1	2.064	51.32	9.204

isentropically. State 26 and state 27 are condensates from the inter-condenser and aftercooler in the form of compressed liquid flowed to the main condenser to be collected and cooled through a cooling tower.

States 28 and 29 are air inlets and outlets of the cooling tower, with the air inhaled using 16 fans at the top of the cooling tower. The fan is driven using a motor with 56 kW of power, and state 30 is fluid from the separator with a liquid phase or brine, which is flowed to the flasher to lower the pressure and temperature. States 31 and 32 are the brines and steams from the results of the estimation in the flasher. This brine is channeled into ponds through canals to precipitate the silica content before injecting it into the earth through injection wells. State 33 is condensate trapped in the CDP, which is discharged into the environment, while state 34 is the scrubber output condensate supplied to the silencer.

The next phase is to analyze the operational data of each state, including pressure (P), temperature (T), and mass flow rate (ṁ). The data was obtained from a daily log sheet in 2019 with an average load of 40.68 MW. The operation data of the Dieng plant in each state are shown in Table 1.

The values of the enthalpy, entropy, energy, and exergy flow rate in each state were conducted using the EES. However, the unavailable parameters were determined using assumptions with heat balance. Based on Table 1, the enthalpy, entropy, energy, and exergy rate in each state were used to analyze the flow rate of the main components, i.e., separator, scrubber, demister, turbine, main condenser, inter-condenser, aftercooler, cooling tower, and flasher.

3. Method

3.1. System Schematic Modelling and Observation Parameters

The schematic of the geothermal power plant system in Dieng is shown in Fig. 1. The parameters utilized include the mass flow rate (ṁ), pressure (P), and temperature (T), with each state consisting of the operation and production log sheet.

3.2. Data and validation

The data is calculated by simulations using the EES. It was carried out to find the value of the enthalpy and entropy in each state. In conducting simulations, it is necessary to perform validation to ensure the results are relevant to the actual situation. The validation was carried out by comparing the enthalpy and entropy values obtained in the EES simulation in each state with the thermodynamic properties in ChemicaLogic Steam and Table A-4 form "Thermodynamics an Engineering Approach" [11], in saturated conditions, the results are obtained as shown in Table 2. Based on these results, almost the same values can be obtained from the EES simulation with the ChemicaLogic Steam application and Table A-4. Thus, it can be seen that the results in the analysis using the EES simulation are quite valid. After the validation results are obtained, the analysis calculations related to energy, exergy, and optimization are carried out to improve the system's performance.

3.3. Energy Analysis

This analysis is conducted in several stages, such as the energy flow rate of each state and component and the calculation of the system's thermal efficiency. The calculation for an energy flow rate of each state is conducted using the following equation 1 [33]. The flow of energy of each component is shown in Table 3.

$$\dot{E}n_{state} = \dot{m}.h_{state} \tag{1}$$

Also, the thermal efficiency is determined using equation 2 [33] as follows:

$$\eta_{thermal} = \frac{\dot{W}_{output}}{Q_{input}} \times 100\% \tag{2}$$

3.4. Exergy Analysis

Exergy analysis is a method based on the second law of thermodynamics used to calculate the amount of irreversibility and exergetic efficiency in a thermal power plant. However, this study uses physical exergy, which is analyzed through several stages, namely, the analysis of the exergy flow rate of each state and component, as well as the analysis of the dead state influence on their exergetic irreversibility and efficiency. The calculation of the exergy rate of each state is based on the following equation 3 [33].

$$\dot{E}_{state} = \dot{m}[(h - h_0) - T_0(s - s_0)] \tag{3}$$

The exergy and irreversibility balance of each component in the Dieng geothermal power plant is shown in Table 4.

Furthermore, the exergetic efficiency of components and systems is determined using equations 4 and 5.

$$\eta_{Exergy} = \left[1 - \left(\frac{\dot{I}}{\dot{E}_{input}}\right)\right] x100\% \tag{4}$$

$$\eta_{System} = \frac{\dot{W}_{output}}{\dot{E}_{input}} \times 100\% \tag{5}$$

The exergy analysis provides information on the component with the highest irreversibility, which is optimized by increasing its exegetic efficiency, resulting in optimal operating conditions.

4. Result and Discussion

4.1. Conversion Process and Analysis

The energy conversion process at the Dieng geothermal power plant is shown through the Temperature-Entropy (T-s) diagram as in Fig. 3. Based on Fig. 3, it is seen that the geothermal fluid in the Dieng is in saturation condition. This fluid emerges from the production well in the form of a mixture of steam and liquid with a fraction of 37.32%. It passes into a separator to separate the steam from the liquid phase at an isobaric pressure of 11 bars. The separated liquid phase flows into the flasher, while the steam phase flows into the scrubber and demister before entering the turbine. The scrubber serves to separate the liquid content carried by steam at a pressure of 8.28 bar, while the demister functions to filter the steam to dry when entering the turbine completely. The steam turbine inlet pressure of 7.5 bar expands to produce power, with its output condensed at a pressure of 0.078 bar.

Table 2
Validation of enthalpy and entropy values in saturated water conditions.

Properties	EES	ChemicaLogic SteamTab Companion	Table A-4 [11]
h (kJ/kg)	188.4	188.435	188.44
s (kJ/kg.K)	0.6385	0.638614	0.6386

Table 3
Energy Flow Rate of Each Component.

Components	Energy Equation Per Component
Separator	$\dot{E}n_{sep} = \dot{E}n_1 - (\dot{E}n_2 + \dot{E}n_{30})$
Scrubber	$\dot{E}n_{scr} = \dot{E}n_3 - (\dot{E}n_4 + \dot{E}n_{34})$
Demister	$\dot{E}n_{dem} = \dot{E}n_5 - \dot{E}n_6$
Turbine	$\dot{E}n_{tur} = \dot{E}n_6 - \dot{E}n_7$
Main Condenser	$_{EnMC} = (\dot{E}n_7 + \dot{E}n_{21} + \dot{E}n_{26} + \dot{E}n_{27}) - (\dot{E}n_8 + \dot{E}n_{13})$
Inter-condenser	$\dot{E}n_{IC} = (\dot{E}n_{14} + \dot{E}n_{23}) - (\dot{E}n_{15} + \dot{E}n_{26})$
After-cooler	$\dot{E}n_{AC} = (\dot{E}n_{16} + \dot{E}n_{25}) - (\dot{E}n_{17} + \dot{E}n_{27})$
Cooling Tower	$\dot{E}n_{CT} = (\dot{E}n_{10} + \dot{E}n_{28}) - (\dot{E}n_{20} + \dot{E}n_{29})$
Flasher	$\dot{E}n_{fla} = \dot{E}n_{30} - (\dot{E}n_{31} + \dot{E}n_{32})$

Table 4
Exergy and irreversibility balance of each component.

Component	Equivalent rate of exergy	Irreversibility
Separator	$\dot{E}_1 = \dot{E}_2+\dot{E}_{30}$	$\dot{E}_1 - (\dot{E}_2+\dot{E}_{30})$
Scrubber	$\dot{E}_3 = \dot{E}_4+\dot{E}_{34}$	$\dot{E}_3 - (\dot{E}_4+\dot{E}_{34})$
Demister	$\dot{E}_5 = \dot{E}_6$	$\dot{E}_5 - \dot{E}_6$
Turbine	$\dot{E}_6 = \dot{E}_7$	$\dot{E}_6 - \dot{E}_7$
Main Condenser	$\dot{E}_7+\dot{E}_{21}+\dot{E}_{26}+\dot{E}_{27} = \dot{E}_8+\dot{E}_{13}$	$(\dot{E}_7+\dot{E}_{21}+\dot{E}_{26}+\dot{E}_{27})$-$(\dot{E}_8+\dot{E}_{13})$
Intercondenser	$\dot{E}_{14}+\dot{E}_{23} = \dot{E}_{15}+\dot{E}_{26}$	$(\dot{E}_{14}+\dot{E}_{23}) - (\dot{E}_{15}+\dot{E}_{26})$
Aftercooler	$\dot{E}_{16}+\dot{E}_{25} = \dot{E}_{17}+\dot{E}_{27}$	$(\dot{E}_{16}+\dot{E}_{25}) - (\dot{E}_{17}+\dot{E}_{27})$
Cooling Tower	$\dot{E}_{10}+\dot{E}_{28} = \dot{E}_{20}+\dot{E}_{29}$	$(\dot{E}_{10}+\dot{E}_{28}) - (\dot{E}_{20}+\dot{E}_{29})$
Flasher	$\dot{E}_{30} = \dot{E}_{31}+\dot{E}_{32}$	$\dot{E}_{30} - (\dot{E}_{31}+\dot{E}_{32})$

Some condensed steams are cooled in the tower, while others are injected into the earth through the wells.

Furthermore, energy analysis is used to determine system performance quantitatively using the First Law of Thermodynamics approach on energy conservation. The quantity of system performance is determined through the amount of energy entering the component, limiting changes. Based on the calculations, each component's energy flow rate values are shown in Table 5.

Table 5 shows the incoming energy flow rate for each component. The separator, scrubber, and demister constantly occur within the system, which decreases its enthalpy and energy. Furthermore, the turbine is a vital component in a power plant. Therefore, its efficiency needs to be calculated. Based on the calculation, the actual work is 45,318 kW, while the isentropic is 57,428 kW. The actual work of the turbine is achieved during the expansion process, while the ideal work is achieved without changes in the isentropic and used to determine its efficiency. The results show that the turbine efficiency is 78.91%, and the system is 10.59%.

Furthermore, the main condenser has an energy rate of 388,217 kW, from steam generated from the turbine and condensed using the water from the cooling tower. Besides, the energy is also extracted from an inter-condenser and aftercooler in the form of condensate. Furthermore, these two components have an energy rate of 12,492 kW and 9,297 kW derived from the ejector's motive steam. This is then discharged into the environment through the cooling tower with an energy rate of 364,848 kW from the main condenser in the form of condensate and ambient air. In principle, the cooling component is used to cool the fluid with the help of the ambient air produced by a fan. The flasher has an energy rate of 122,693 kW originating from the brine, which results from the separator.

In general, energy analysis only shows the amount of incoming energy that changes due to a decrease in enthalpy. However, not all of these amounts of energy are converted into work. Therefore, this research also discusses the exergy analysis to determine the cause of the enthalpy decrease in each state and also considers the value of entropy growth based on the second law of thermodynamics. The results of this analysis are used as a reference for the optimization and improvement of efficiency.

Exergy analysis is carried out to determine the size, location, and causes of irreversibility in the main components of the plant. This study only figures out the physical exergy because it has no combustion process. The results are shown in Fig. 4.

The flow of exergy is the availability of energy used in a process. In Fig. 4 shows the total exergy of each component. In this case, a decrease of exergy which enters the scrubber indicates that those from the separator are damaged due to irreversibility. It is also influenced by condensation during the distribution from the gathering system to the scrubber, where 5.89% of the mass flow rate is condensed and drained via the CDP contained in the steam line. Another cause of the decrease is the separation process between the steam phases with the liquid in the separator, where the water flows into the flasher.

Furthermore, around 70,881 kW of exergy entering the demister is reduced compared to the scrubber by 73,650 kW. Besides being influenced by the irreversibility of the scrubber, the steam is ejected in the 1st

Table 5
Energy Flow Rate of Each Component.

Component	Energy Flow Rate (kW)
Separator	384226
Scrubber	243583
Demister	234533
Turbine	234189
Main Condenser	388217
Intercondenser	12492
Aftercooler	9297
Cooling Tower	364848
Flasher	122693

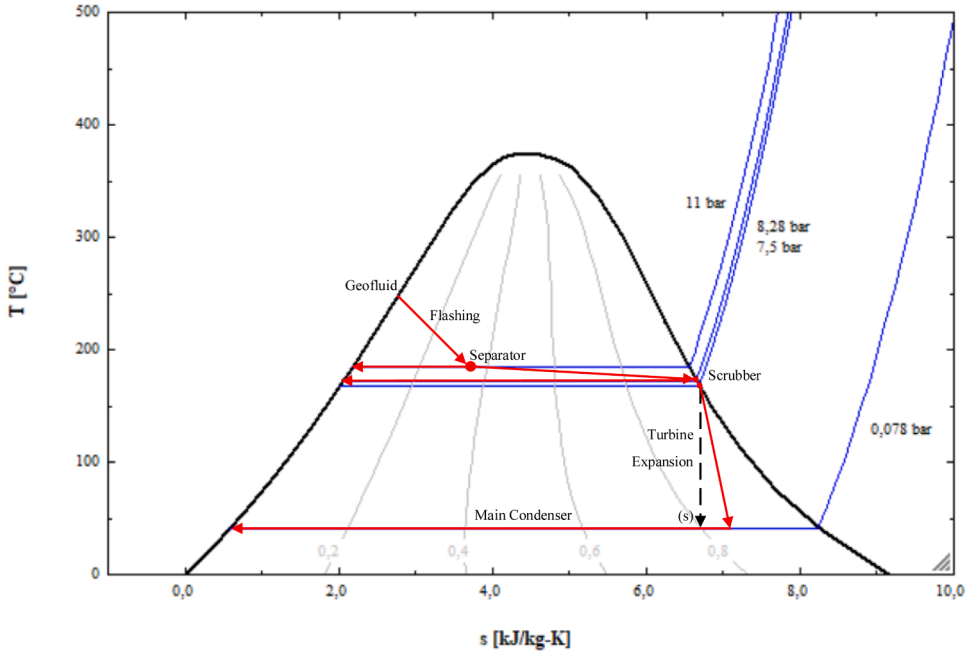

Fig. 3. Temperature-Entropy (T-s) Diagram

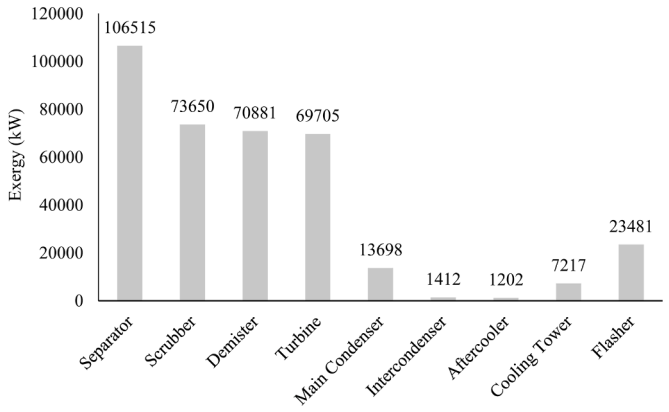

Fig. 4. Total Exergy of Each Component

and 2nd ejectors. Approximately 69,705 kW exergy enters the turbine to produce 40,680 kW, which decreases due to the irreversibility of the demister. The next component is the main condenser with an exergy amount of 13,698 kW, which is the output of the turbine after the expansion process and the exergy of the inter-condenser and aftercooler.

The inter-condenser component has total exergy of 1,412 kW originating from motive steam with a part adsorbed from the main condenser. In contrast, the exergy originating from NCG in this study is ignored, as explained in the previous section. Furthermore, the aftercooler has an exergy amount of 1,202 kW, which also comes from the motive steam sucked from the intercondenser during the NCG extraction process.

The next component is the cooling tower with an exergy amount of 7,217 kW generating from the condensate. The last component is the flasher which has exergy of 23,481 kW derives from the separator. At the same time, the location and magnitude of irreversibility are determined by calculating the irreversibility of each component of the geothermal power plant, as seen in Fig. 6.

From Fig. 5, it can be seen that the greatest exergy extermination occurred in the turbine by 11217 kW, 7808 kW condenser, 6056 kW flasher, 5087 kW separator, 2428 kW cooling tower, 1176 kW demister, 1007 kW intercondenser, 868.5 kW aftercooler, and a scrubber of 44.48 kW. Extermination of exergy in these components comes from several major irreversibilities, including heat transfer and friction between the fluid and the components. To explain the cause of irreversibility, as mentioned above, the amount of exergy in and out of each component is presented in Table 6.

Table 6 described the total exergy in and out of each component, as well as the irreversibility and cause. Also, the exergetic efficiency of each component is shown in Fig. 6.

Table 6
Total Exergy in and Out of Each Component.

Component	E_{input} (kW)	E_{output} (kW)
Separator	106515	101428
Scrubber	73650	73605
Demister	70881	69705
Turbine	69705	58488
Main Condenser	13698	5890
Intercondenser	1412	405,2
Aftercooler	1202	333,1
Cooling Tower	7217	4790
Flasher	23481	17425

Based on Fig. 6, the separator, scrubber, and demister consist of exergetic efficiency above 95%, which indicates that the components do not lose much exergy. The turbine has an exergetic efficiency of 83.91%, which depreciates during the expansion process. Also, the main condenser, intercondenser, and aftercooler have an exergetic efficiency of 43%, 28.69%, and 27.72%, while that of the cooling tower is equal to 66.36%. Furthermore, the flasher has an exergetic efficiency of 74.21%.

The Sankey diagram in Fig. 8 provides a very clear picture of the amount of exergy entering the system as well as the exergy loss in each component of the geothermal power plant.

The Sankey diagram is used to provide a clearer picture of the exergy flow. Based on Fig. 7, the total exergy flow that enters the system is 106,515 kW. However, not all are converted into electricity due to destruction resulting from irreversibility in the components. Fig. 6 shows the amount of exergy loss in separators, scrubbers, and demisters by 4.78% or 5087 kW, 0.04% or 44.48 kW, and 1.10% or 1176 kW, respectively. Other components such as the turbine, main condenser, and intercondenser experience exergy loss by 10.53% or 11,217 kW, 7.33% or 7,808 kW, and 0.95% or 1,007 kW. While, in the aftercooler, cooling tower, and flasher, there was an exergy loss by 0.82% or 868.5 kW, 2.28% or 2428 kW, and 5.69% or 6056 kW. The total exergy converted into electricity is 70,824 kW or 66.49% of the total reserves that enter the system.

4.2. Exergy Optimization

This section describes the optimization efforts performed on turbines as the components with the greatest irreversibility. It was conducted by determining the ambient temperature to obtain optimal operating conditions and increasing its exergetic efficiency, reducing the irreversibility. The optimization is carried out by adjusting the turbine inlet pressure to its specifications and setpoints regulated by the company, namely, 5.5, 6, 6.5, 7, 7.5, and 8 bars. EES conducted it with the applied mass of 40.68 MW. The results are shown in Fig. 8 as follows.

Based on Fig. 8, it is explained that the higher turbine inlet pressure increases its irreversibility and decreases the exergetic efficiency. It

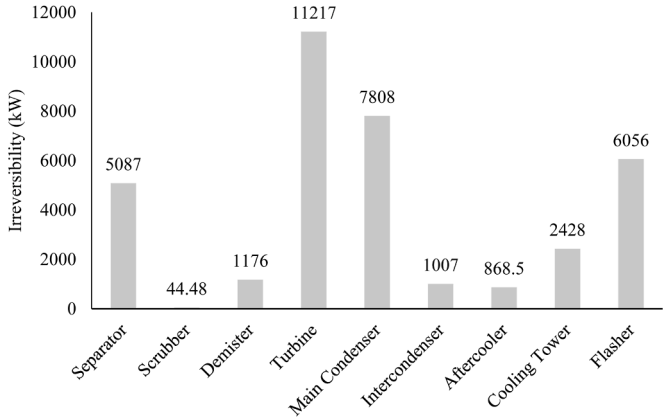

Fig. 5. Irreversibility of Each Component

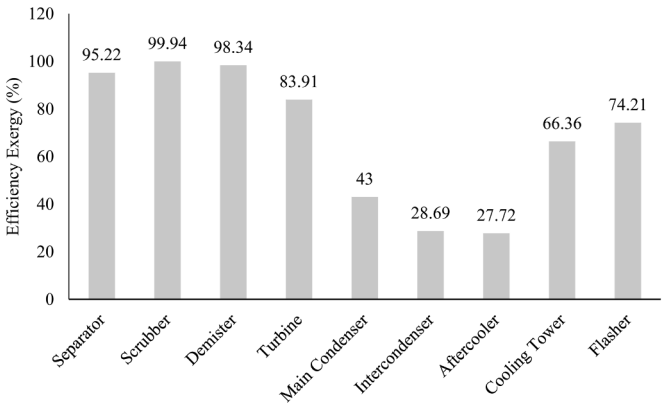

Fig. 6. Exergetic Efficiency of Each Component

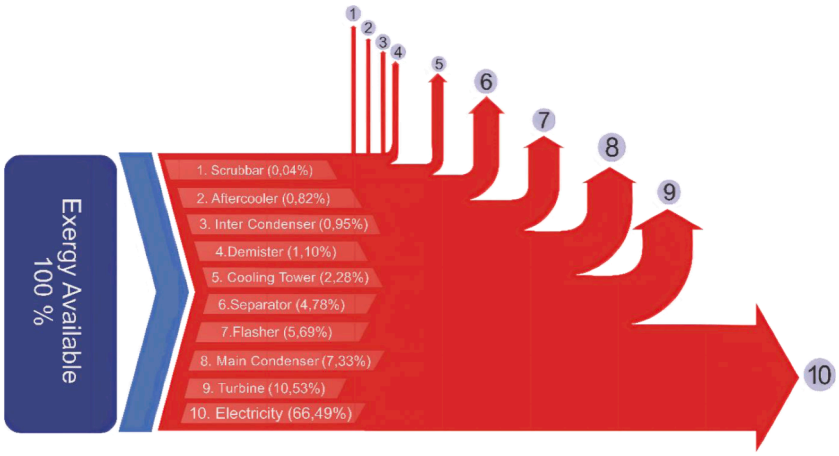

Fig. 7. Sankey Diagram of exergy flow

causes greater inlet exergy, thereby producing constant 40.68 MW power output. When the inlet exergy value is bigger, the power output value remains constant, thereby decreasing the exergetic efficiency. Therefore, the exergy destruction on the governor should keep the stability of turbine rotation at 3000 rpm to obtain the generator frequency of 50 Hz.

Fig. 8 also shows the optimal operating at each ambient temperature. It is a condition with high exergetic efficiency and low irreversibility. At an ambient temperature of 16°C, the optimal operating conditions are in the pressure range of the 5.5-7.2 bar. However, when it exceeds the maximum pressure limit, it tends to increase the irreversibility and lower the exergetic efficiency, as the opposite of the optimal condition. Furthermore, when the ambient temperature is 17°C and 18°C, the optimal conditions are in the pressure ranges of 5.5-6.9 bar and 5.5-6.6 bar, respectively. The ambient temperature is 19°C and 20°C. The optimal operating condition is in the pressure ranges of 5.5-6.3 bar and 5.5-6 bar, respectively. Based on these pressure ranges, it is concluded that the higher the ambient temperature, the lower the maximum pressure of the turbine inlet under optimal operating conditions and vice versa. This indicates that the higher exergy is destroyed with an increase in ambient temperature, leading to greater component irreversibility.

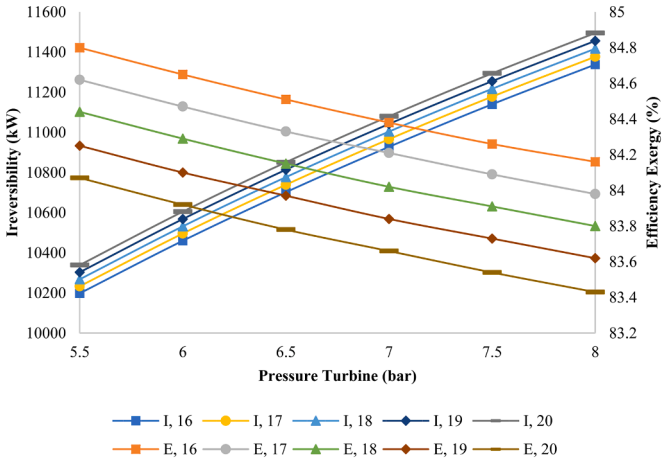

Fig. 8. Effect of Pressure on Irreversibility and Exergetic Efficiency

5. Conclusion

Geothermal energy is a potentially renewable resource, which can be utilized directly or through a sustainable prior process, and produces minimal emissions. Based on the analysis results in this study, it can be concluded that Energy analysis provides information on its flow rate in each component of the geothermal power plant without considering entropy and ambient conditions. While the exergy analysis provides information on the greatest irreversibility in the turbine of 11217 kW, 7808 kW main condenser, 6056 kW flasher, 5087 kW separator, and cooling tower of 2428 kW. Other components such as the demister, intercondenser, aftercooler, and scrubber have no significant irreversibility of 1176 kW, 1007 kW, 868.5 kW, and 44.48 kW, respectively. Besides, the exergy analysis results acquired the exergetic efficiency of each component with the 95.22%separator, 99.94% scrubber, 98.34% demister, 83.91%turbine, 43% main condenser, 69% intercondenser, 27.72% aftercooler, 66.36% cooling towers, and 74.21% flasher.

The ambient temperature affects the irreversibility and exergetic efficiency of each component. The higher the ambient temperature, the lower the system's irreversibility, which increases the exergetic efficiency and vice versa. Furthermore, exergy optimization is carried out on the inlet turbine due to its high irreversibility in the geothermal power plant system. The optimization shows that the higher the inlet pressure, the higher its irreversibility rate and the lower the turbine exergetic efficiency. Finally, the optimal turbine inlet pressure was obtained at a pressure of 5.5 bar, with the maximum pressure changing following the ambient temperature.

Declaration of Competing Interest

The authors declare that they have no known competing financial interests or personal relationships that could have appeared to influence the work reported in this paper.

Acknowledgment

Our thanks to the Directorate General of Higher Education, Ministry of Research, Technology and Higher Education, Republic of Indonesia. This grant was given by MIRA (MIT-Indonesia Research Alliance) in 2019.

Reference

[1] Ministry of Energy and Mineral Resources, 2017. Potensi Panas Bumi Indonesia Jilid 1. Kementerian Energi dan Sumber Daya Mineral, Jakarta.
[2] Sudarman, S., Hochstein, M.P., 2017. History of Geothermal Exploration in Indonesia (1970-2010). In: Proceedings 36th New Zealand Geothermal Workshop 24 - 26 November 2014 no. January.
[3] Nasruddin, N., Alhamid, M.I., Daud, Y., Surachman, A., Sugiyono, A., 2020. Potential of geothermal energy for electricity generation in Indonesia: A review. Renew. Sustain. Energy Rev. 53 (2016), 733–740. https://doi.org/10.1016/j.rser.2015.09.032.

[4] Prasetio, R., Abidin, Z., Yulizar, Y., 2010. Isotope and Gas Geochemistry of Dieng Geothermal Field, Indonesia, pp. 25–29. April.
[5] Mohammadzadeh, S., Jalilinasrabady, S., Fujii, H., Pambudi, N.A., 2018. Classification of geothermal resources in Indonesia by applying exergy concept. Renew. Sustain. Energy Rev. 93 (May), 499–506. https://doi.org/10.1016/j.rser.2018.05.018.
[6] Kamila, Z., Kaya, E., Zarrouk, S.J., 2021. Reinjection in geothermal fields: An updated worldwide review 2020. Geothermics 89 (June 2020), 101970. https://doi.org/10.1016/j.geothermics.2020.101970.
[7] Bejan, A., Tsatsaronis, G., Moran, M., 1996. Thermal Design and Optimization. John Wiley & Sons, Inc, New York.
[8] Bejan, A., 1996. Entropy Generation Minimization. CRC Press, New York.
[9] Dincer, I., Rosen, M.A., 2007. Exergy: Energy, Environment, and Sustainable Development. Elsevier Ltd, Canada.
[10] Nasruddin, N., Dwi Saputra, I., Mentari, T., Bardow, A., Marcelina, O., Berlin, S., 2020. Exergy, exergoeconomic, and exergoenvironmental optimization of the geothermal binary cycle power plant at Ampallas, West Sulawesi, Indonesia. Therm. Sci. Eng. Prog. 19 (June), 100625 https://doi.org/10.1016/j.tsep.2020.100625.
[11] Cengel, Y.A., Boles, M.A., 2015. Thermodynamics An Engineering Approach, 8th ed. McGraw-Hill Education, New York.
[12] Shukuya, M., Hammache, A., 2002. Introduction to the Concept of Exergy - for a Better Understanding of Low - Temperature - Heating and High - Temperature - Cooling Systems. VTT Tiedotteita.
[13] Yumrutaş, R., Kunduz, M., Kanoğlu, M., 2002. Exergy analysis of vapor compression refrigeration systems. Exergy, An Int. J. 2 (4), 266–272. https://doi.org/10.1016/s1164-0235(02)00079-1.
[14] Pambudi, N.A., Itoi, R., Jalilinasrabady, S., Jaelani, K., 2014. Exergy analysis and optimization of Dieng single-flash geothermal power plant. ENERGY Convers. Manag. 78, 405–411. https://doi.org/10.1016/j.enconman.2013.10.073.
[15] Pambudi, N.A., Itoi, R., Jalilinasrabady, S., Jaelani, K., 2015. Performance Improvement of Single-Flash Geothermal Power Plant Applying Three Cases Development Scenarios Using Thermodynamic Methods Performance Improvement of Single-Flash Geothermal Power Plant Applying Three Cases Development Scenarios Using Thermodyn. In: Proc. World Geotherm. Congr. Melbourne, Aust. 19-25 April 2015. April.
[16] Rudiyanto, B., Illah, I., Agung, N., Cheng, C., 2017. Preliminary analysis of dry-steam geothermal power plant by employing exergy assessment: Case study in Kamojang geothermal power plant, Indonesia. Case Stud. Therm. Eng. 10 (May), 292–301. https://doi.org/10.1016/j.csite.2017.07.006.
[17] Setyawan, N.D., et al., 2018. Energy and exergy analysis of dry-steam geothermal power plant: Case study in kamojang geothermal power plant unit 2. In: AASEC 2018, 08018, pp. 1–5. https://doi.org/10.1051/matecconf/201819708018.
[18] Unverdi, M., Cerci, Y., 2013. Performance analysis of Germencik Geothermal Power Plant. Energy 52, 192–200. https://doi.org/10.1016/j.energy.2012.12.052.
[19] Yari, M., 2010. Exergetic analysis of various types of geothermal power plants. Renew. Energy 35 (1), 112–121. https://doi.org/10.1016/j.renene.2009.07.023.
[20] Ghazvini, M., Sadeghzadeh, M., Ahmadi, M.H., Moosavi, S., Fathollah, P., 2019. Geothermal energy use in hydrogen production: A review. Int. J. Energy Res. (April), 1–29. https://doi.org/10.1002/er.4778.
[21] Koroneos, C., Polyzakis, A., Nanaki, E., Xydis, G., Stylos, N., October 2016. Exergy analysis for a proposed binary geothermal power plant in Nisyros Island, Greece. Geothermics 2017.
[22] Dipippo, R., 2013. Geothermal double-flash plant with interstage reheating: An updated and expanded thermal and exergetic analysis and optimization. Geothermics 48, 121–131. https://doi.org/10.1016/j.geothermics.2013.07.006.
[23] Jalilinasrabady, S., Itoi, R., Valdimarsson, P., Saevarsdottir, G., Fujii, H., 2012. Geothermics Flash cycle optimization of Sabalan geothermal power plant employing exergy concept. Geothermics 43, 75–82. https://doi.org/10.1016/j.geothermics.2012.02.003.
[24] A. Dagdas, R. Ozt, and S. Bekdemir, "Thermodynamic evaluation of Denizli Kızıldere geothermal power plant and its performance improvement," vol. 46, pp. 245–256, 2005, doi: 10.1016/j.enconman.2004.02.021.
[25] Coskun, C., Oktay, Z., Dincer, I., 2011. Performance evaluations of a geothermal power plant. Appl. Therm. Eng. 31 (17–18), 4074–4082. https://doi.org/10.1016/j.applthermaleng.2011.08.013.
[26] Y. Basogul, "Environmental assessment of a binary geothermal sourced power plant accompanied by exergy analysis," vol. 195, no. May, pp. 492–501, 2019, doi: 10.1016/j.enconman.2019.05.033.
[27] Wan, P., Gong, L., Bai, Z., 2019. Thermodynamic analysis of a geothermal-solar flash-binary hybrid power generation system. Energy Procedia 158, 3–8. https://doi.org/10.1016/j.egypro.2019.01.023.
[28] H. Gokgedik, M. Yürüsoy, and A. Keçebas, "Improvement potential of a real geothermal power plant using advanced exergy analysis," vol. 112, pp. 254–263, 2016, doi: 10.1016/j.energy.2016.06.079.
[29] B. Yuksel, A. Aslan, and T. Akyol, "Investigation of seasonal variations in the energy and exergy performance of the Gonen geothermal district heating system," vol. 36, no. February 2004, 2012, doi: 10.1016/j.applthermaleng.2011.12.003.
[30] Budisulistyo, D., Krumdieck, S., 2015. Thermodynamic and economic analysis for the pre-feasibility study of a binary geothermal power plant. Energy Convers. Manag. 103, 639–649. https://doi.org/10.1016/j.enconman.2015.06.069.
[31] Atiz, A., Karakilcik, H., Erden, M., Karakilcik, M., 2019. Investigation energy, exergy and electricity production performance of an integrated system based on a low-temperature geothermal resource and solar energy. Energy Convers. Manag. 195 (May), 798–809. https://doi.org/10.1016/j.enconman.2019.05.056.
[32] Junaldi, Indriawati, K., 2012. Prediction of Electric Power Geothermal Power Plant Based on the Weighted Moving Average Method at PT. GEO DIPA ENERGI Dieng Unit. J. Tek. Pomits 1 (1), 1–6 [Online]. Available: http://digilib.its.ac.id/public/ITS-paper-23173-2408100012-Paper.pdf.
[33] Moran, M.J., Saphiro, H.N., 2006. Fundamentals of Engineering Thermodynamics, 5th ed. John WIley & Sons, Inc., West Sussex, England.